Investigating sulfide-based all solid-state cells performance through P2D modelling

Chemical Engineering Journal Advances 18 (2024) 100610

Contents lists available at ScienceDirect

Chemical Engineering Journal Advances

journal homepage: www.sciencedirect.com/journal/chemical-engineering-journal-advances

# Investigating sulfide-based all solid-state cells performance through P2D modelling

D. Dessantis [a], P. Di Prima [a], D. Versaci [b], M. Santarelli [a], F. Bella [b], V. Kolotygin [c], P. López-Aranguren [c], J. Amici [b,*]

[a] Synergy of Thermo-chemical and Electro-chemical Power Systems (STEPS), Department of Energy, Polytechnic of Turin, corso Duca degli Abruzzi 24, 10129, Turin, Italy
[b] Electrochemistry Group, Department of Applied Science and Technology, Polytechnic of Turin, corso Duca degli Abruzzi 24, 10129, Turin, Italy
[c] Centro de Investigación Cooperativa de Energías Alternativas (CIC energiGUNE) Basque Research and Technology Alliance (BRTA), Parque Tecnológico de Àlava Albert Einstein 48, 01510, Vitoria-Gasteiz, Spain

ARTICLE INFO

*Keywords:*
All solid-state battery
Metallic lithium
Solid-State Electrolyte
Argyrodite
P2D modelling

ABSTRACT

All solid-state batteries, combining metallic lithium with a solid-state electrolyte, are now considered as a very promising answer to the growing need for higher energy density in safer batteries. While research interests are quickly raising on this topic, the number of experiments to perform in order to find the best combination of active material and solid electrolyte composition could be infinite. Therefore, an easy and low computational-cost model forecasting all solid-state cells performance could accelerate the optimization and lower the number of experiments, reaching more rapidly an up scalable solution.

In this work, an innovative electrochemical model for a metallic lithium – argyrodite $Li_6PS_5Cl$ – NMC622 cell is developed. In particular, two important aspects, characterizing this new battery generation, are implemented inside a P2D model.

The first aspect is the implementation of a solid-state electrolyte, in substitution to liquid electrolyte, which means using the single ion conducting electrolyte theory, according to which Ohm's law is the only equation to be solved in the electrolyte domain. This reduces the number of parameters characterizing the electrolyte from three, for the liquid electrolyte (ionic conductivity, transference number, and mean molar activity coefficient), to only one, for the solid electrolyte (ionic conductivity). The second aspect regards the anode side, lithium metal is chosen, in substitution to graphite, and this implies a different treatment from an electrochemical point of view, which is to consider the anode as a boundary condition instead of a porous electrode. Such drastic simplification of the P2D model allows, after careful calibration and validation based on experimental data, to obtain reliable charge/discharge profiles at C/10 and C/5 for lithium – argyrodite $Li_6PS_5Cl$ – NMC622 cells.

## 1. Introduction

The increase in the use of energy based on fossil fuels, caused by population growth, has led to the depletion of these energy resources and global warming. [1–3] Therefore, new forms of renewable and sustainable energy must be identified and developed. Due to the sporadic nature of renewable energy, it is necessary to develop efficient energy storage systems, capable of storing and supplying energy when needed. [4] Because of the smallest ionic radii of lithium (Li) and the lowest reduction potential, Li-ion batteries (LIBs) have been chosen as the most promising battery system to reach high gravimetric/volumetric energy and power densities. [5] In fact, in recent years, LIBs have been used in various everyday devices such as laptops, mobile phones and electric vehicles. [6–8] However, present commercial LIBs are reaching their theoretical limits (680 Wh $L^{-1}$ and 250 Wh $kg^{-1}$) [9,10]. One of the main causes is the use of graphite as anode, which limits the increase in LIBs energy density due to its low theoretical volumetric and specific capacities (735 mAh $cm^{-3}$ and 372 mAh $g^{-1}$, respectively) [11]. Metallic Li represents an interesting alternative to graphite thanks to its extremely high theoretical volumetric and gravimetric specific capacities (2061 mAh $cm^{-3}$ and 3860 mAh $g^{-1}$, respectively). [12,13] Hence, Li-metal batteries (LMBs) with high-voltage cathodes, or as Li-S and

* Corresponding author.
*E-mail address:* julia.amici@polito.it (J. Amici).

https://doi.org/10.1016/j.ceja.2024.100610
Received 16 February 2024; Received in revised form 27 March 2024; Accepted 10 April 2024
Available online 16 April 2024

Li-$O_2$ batteries, can be seen as auspicious devices for the future generation of high-energy rechargeable batteries. [14–16] Unfortunately, Li metal anode (LMA) suffers from some drawbacks, [17,18] such as the formation of lithium dendrites, which can affect the battery safety. [19–23] Moreover, the continuous consumption of liquid electrolyte to re-form the solid electrolyte interphase (SEI), breaking upon dendrites growth, affects the galvanostatic cycling performances of LMBs. [24–26, 18]

Various strategies have been studied and employed to solve the LMA issues, such as the construction of an artificial SEI layer [27,28], the insertion of additives in liquid electrolytes [29–31], and the use of alternative electrolytes that can substitute the commercial liquid electrolytes. [32] Considering this latter strategy, solid-state electrolytes (SSEs) represent an optimal solution for the design of safe solid-state batteries using LMA. [33] Replacing a liquid electrolyte by a SSE, which works as well as separator, would design a solid and more tolerant system towards Li metal, that could mitigate the issues of LMBs previously mentioned. [34] Therefore, the all-solid-state batteries (ASSBs) can be considered as the future generation of LMBs. [35]

Solid-state electrolytes are usually divided into two main categories: polymer electrolytes and inorganic electrolytes. [36] Polymer electrolytes possess some peculiar characteristics: lightness, flexibility, and the possibility to control the thickness using standard preparation techniques as pressing or extrusion [37–39], but their main disadvantages are the low mechanical strength and electrode compatibilities. [40,41]. On the other hand, inorganic electrolytes can be classified into two sub-categories: oxides and sulfides. [42] Inorganic oxide electrolytes comprise Lithium SuperIonic CONductor (LiSICON), Lithium aluminium Titanium Phosphate (LATP) and Lithium Phosphorous Oxy-Nitride (LiPON). [43] The first one is characterized by low reactivity towards moisture but shows poor ionic conductivity (around $10^{-7}$ S $cm^{-1}$) at ambient temperature. [44] LATP-based electrolytes present a wide electrochemical window, up to 6 V, and an ionic conductivity of $7 \times 10^{-4}$ S $cm^{-1}$, [45] while LiPON electrolytes display an intermediate behaviour between LATP and LiSiCON with an ionic conductivity of $2 \times 10^{-6}$ S $cm^{-1}$. [46] The second class of inorganic electrolytes, the sulfides, possesses higher values of ionic conductivity (up to $2.5 \times 10^{-2}$ S $cm^{-1}$) than the oxides, due to the larger size and higher polarizability of sulfur with respect to oxygen. [47,48] It is possible to define two sub-categories of sulfides: amorphous (glassy) and crystalline (glass--ceramic). [49,50] The amorphous sulfide electrolytes are ductile, but require elevated temperatures during the assembly of the cell in order to avoid the crystallization. Sulfide crystalline electrolytes (thio-LiSICON) are usually represented with the formula $Li_xM_{1-\delta}M_\delta'S_4$, where M represents Si, Ge, or Sn, while M' represents P, Ga, Al, or Zn. [51,52] Inside this category, the most famous electrolytes are argyrodite-type-ones $Li_6PS_5X$ ($X$ = $I$, Cl, Br). [53–55] Unfortunately, even if ASSBs with LMA represent a suitable alternative to commercial LIBs, at the moment they suffer from some issues, such as: a) weak physical contact between the cathode active material and the SSE, [56] b) the high internal resistance at the interface between the electrodes and the SSE, [57–59] c) surface defects and the existence of grain and grain boundaries inside the microstructure of SSE, [60] and d) the narrow electrochemical stability window against anodic and cathodic materials. [61–63] These problems can affect the safety of ASSBs, bringing to lithium metal penetration and internal short circuit. [64,65]

Thus, considering the several matters that influence the electrochemical performance of ASSB with metallic lithium anode, modelling represents an interesting and robust tool for examining this future generation of batteries. [66,67] In fact, the use of modelling can provide a support to better understand the mechanisms that occur at the interface [68] so as to improve the electrochemical performance of LMB with SSE. [69] Depending on the spatial scale, different multiscale models have been studied and developed with the aim to study the behaviour and the mechanisms that characterize LIBs. [70–73] In particular, macroscale models are useful to improve the electrochemical behaviour of LIBs by analysing the effects of electrochemical parameters variations on battery performances. Such models can be divided into three sub-categories: equivalent circuit, empirical, and electrochemical. [74] As reported by several works, the electrochemical models are a practical and state-of-the-art tool for battery state estimation, reaction mechanistic analysis and battery design optimization. [75] The pseudo-two-dimensional (P2D) model, based on concentrated solution theory, porous electrode theory, and kinetics equation, developed by Fuller, Doyle, and Newman, is one of the most useful electrochemical models available in literature. [76] The main feature of the P2D model is the high degree of accuracy due to the precise representation of the electrode microstructure. [77,78] In fact, the P2D model describes the microstructure using spherical particles with the same radius and solving the one-dimensional diffusion-based transport equation in the particles. [79] Some studies have already implemented the LMA in an electrochemical model [80,81], also considering new battery chemistries, such as Li-S [82,83] and Li-air [84,85], while other models have described how to consider solid-state electrolyte in substitution of liquid electrolyte [86]. However, to the best of our knowledge, no P2D models combining a SSE with the LMA, against a NMC622 cathode, have not been reported yet.

Therefore, in this study, with the help of the commercial software COMSOL Multiphysics, a P2D electrochemical model was developed for a cell containing Li metal as anode and argyrodite $Li_6PS_5Cl$ as solid-state electrolyte. Nickel Manganese Cobalt ($LiNi_{0.6}Mn_{0.2}Co_{0.2}O_2$, shortened as NMC622) was selected as cathode active material because of the good compatibility with argyrodite SSE, as reported in previous studies, [87, 88] together with the fact that it represents a good compromise between high energy density and low cobalt content. Therefore, properly coupled with a Li metal anode it should allow to reach higher energy density. Experimental characterizations were performed in order to obtain precise electrochemical parameters to calibrate thoroughly the model. It was, successively validated through a comparison between the simulated and the experimental charge-discharge cycles at several C-rates. The optimal comparison between the simulated and the experimental curves confirms the robustness of the chosen approach and the innovation of the model developed combining metallic lithium with SSE. Last but not least, another important advantage of the electrochemical model developed is the low computational cost, because two to three days of experimental testing (1 charge-discharge cycle at C/30) can be simulated in less than half an hour.

## 2. Modelling

### 2.1. P2D model

LIBs have been extensively studied through the P2D electrochemical model due to its high accuracy, good accordance with the experimental data, and its little computational cost. Therefore, a P2D concept was utilized in the development of an electrochemical model with the purpose to characterize and foresee the electrochemical behaviour of a LMA battery with a SSE. The acronym P2D is referred to two different 1D dimensions: the first dimension is the thickness of the cell, and the second one is the one of the active material spherical particles. Regarding the cell thickness, the electrochemical device was modelled dividing it in four sub-domains, which represent the metallic Li as anode, the argyrodite as SSE, NMC622 as cathode, and aluminium as current collector, respectively.

The current collector is modelled through Ohm's law (Eq. (1)), because it can be seen as a non-reacting electrode where the only physical phenomenon considered is electronic conduction. In Eq. (1), $i_s$ is the local current density, $\sigma_s$ is the electrical conductivity of aluminium, and $\phi_s$ is the electrode potential.

$$i_s = -\sigma_s \nabla \phi_s \tag{1}$$

For the cathode, Eq. (2) describes the mechanism of $Li^+$ insertion into

the electrode active material. Here, $i_{tot}$ expresses the total current density passing through the electrode, under the influence of a certain number of reactions (NR), while $i_{loc,i}$ is the current density generated by the i$^{th}$ reaction in the electrode.

$$i_{tot} = \sum_{i=1}^{NR} a_{v,i} i_{loc,i} \tag{2}$$

$a_v$ is defined as the specific surface electrode and can be computed according to Eq. (3), where $m$ is the geometric factor (usually $m = 3$ for spherical particles), $\varepsilon_s$ is the active volume fraction, and $r_p$ is the radius particle.

$$a_v = \frac{m\varepsilon_s}{r_p} \tag{3}$$

Butler-Volmer equation (Eq. (4)) is adopted to describe the chemical kinetics of the lithium-ion reaction with the electrode active material. In Eq. (4), $i_0$ is the exchange current density, $\alpha_a$ and $\alpha_c$ are the anodic and cathodic charge transfer coefficients, $\eta$ is the surface over-potential, F, R and T represent Faraday's constant, the universal gas constant, and the temperature, respectively.

$$i_{loc} = i_0 \left[ exp\left(\frac{\alpha_a F\eta}{RT}\right) - exp\left(\frac{-\alpha_c F\eta}{RT}\right) \right] \tag{4}$$

The pores tortuosity and the presence of the SSE increasing transport distance, a reduced conductive material volumetric fraction in the electrode should be considered. It is therefore possible to define "effective" values for electrolyte and electrode conductivities. In the study, the Bruggeman's relationship is considered, defining tortuosity as a function of the material porosity. The effective conductivity of the solid phase $\sigma_{s,eff}$ and the effective conductivity of the electrolyte phase $\sigma_{l,eff}$ can be computed through Eq. (5), in which $\tau_l$ and $\varepsilon_p$ represent the tortuosity and the porosity of the material, respectively.

$$\tau_{l,Brug} = \varepsilon^{-0,5} \rightarrow \begin{cases} \sigma_{l,eff} = \varepsilon_p^{1,5}\sigma_l \\ \sigma_{s,eff} = \varepsilon_p^{1,5}\sigma_s \end{cases} \tag{5}$$

Fick's law (Eq. (6)) is used to characterize the diffusion of $Li^+$ in the active material, along the radial dimension of the particles, using boundary conditions described by Eq. (7).

$$\frac{\partial c_s}{\partial t} = \nabla(-D_s \nabla c_s) \tag{6}$$

$$\frac{\partial c_s}{\partial r} = 0|_{r=0} \quad -D_s \frac{\partial c_s}{\partial r} = -\frac{\nabla i_s}{a_v F}|_{r=r_p} \tag{7}$$

### 2.2. Solid-state electrolyte model

For the modelling of the SSE, the same approach suggested by Wolff et al. [86] was implemented in the P2D electrochemical model developed. In their work, single ion conducting electrolyte theory is considered, according to which only one charged species (Li-ion) is mobile, whereas in a cell with binary electrolyte both $Li^+$ and the counterion are mobile. With the assumption of only one mobile species and electroneutrality ($\sum z_k c_k = 0$), there is no concentration gradient within the electrolyte, as stated by Eq. (8):

$$\frac{\partial c_l}{\partial t} = 0 \tag{8}$$

Since there is no concentration gradient in the electrolyte, the electrolyte conductivity $\sigma_l$ does not vary with spatial coordinate. Therefore, adopting the single ion conducting electrolyte theory, the electrolyte potential drop can be described by Ohm's law (Eq. (10)) simplifying the equation usually adopted for liquid electrolyte current density (Eq. (9)):

$$i_l = -\sigma_l \nabla\phi_l + \frac{2\sigma_l RT}{F}\left(1 + \frac{\partial lnf}{\partial lnc_l}\right)(1 - t_+)\nabla c_l \tag{9}$$

$$i_l = -\sigma_l \nabla\phi_l \tag{10}$$

### 2.3. Lithium metal model

Lithium metal is considered as an infinite reservoir of lithium, as such it has no dimension, and is therefore considered a boundary. [80] The lithium electrode is assumed as ideal, hence a Butler-Volmer equation, similar to Eq. (4), can be considered [81,89].

The over-potential, due to the electrochemical reaction, can be expressed by Eq. (11), in which $\phi_l$ is the electrolyte potential, and the OCV function represents the cell open-circuit potential varying with the State of Charge (SoC).

$$\eta = \phi_s - \phi_l - OCV(SoC) \tag{11}$$

Two different boundary conditions are used in this electrochemical model.

The first one is the boundary condition "ground", it corresponds to Eq. (12), and it is applied to define a reference potential within the model. In this work, this boundary condition is applied at the metallic lithium negative electrode, to define the cell voltage according to Eq. (13).

$$\phi_s = 0 \tag{12}$$

$$E_{cell} = \phi_{s,cathode} - \phi_{s,anode} \tag{13}$$

The second one is the boundary condition "charge-discharge cycle", it is applied at the end of the positive current collector, in order to model the cell galvanostatic cycling behaviour. Following experimental protocol, cell charging corresponds to a positive current, up to a maximum cut-off voltage (4.2 V), while, cell discharging corresponds to a negative current down to the minimum cut-off voltage (2.7 V).

## 3. Experimental section

The validation of the P2D electrochemical model described in the previous section consists of comparing the simulated charge-discharge curves and the experimental ones at different C-rates. Thus, LMA batteries with SSE must be assembled adopting the same configuration described in the electrochemical model: Li metal as anode, argyrodite $Li_6PS_5Cl$ as solid-state electrolyte, NMC622 as cathode, and aluminium as current collector. Despite this, a calibration of the model is necessary before going on with the final validation of the same. The calibration step consists in fitting the electrochemical model to the experimental results: therefore, it is useful to evaluate some electrochemical parameters through experimental measurements with the final purpose to perform modelling simulation as much realistic as possible. In this section, the preparation of the electrodes and the solid-state electrolyte, the assembly of the coin cells, and the cycling protocols adopted for the experiments and the calibration will be accurately described.

### 3.1. Electrode and solid-state electrolyte preparation and coin cell assembly

Solid electrolyte (SE) pellets were prepared in a Ø6 mm press die. 30-40 mg electrolyte powders were sequentially pressed at 300–450-600 MPa, maintaining the pressure for 2 min per each step. For the preparation of cathode slurries, the cathode mixture of NMC622, SE, and C65 (C—NERGY™ Super C65, Imerys) in a mass ratio of 67.4 : 28.2 : 4.4 respectively, was dispersed in toluene (solid : liquid ≈ 1:1.4 wt.%), followed by the addition of 5 wt.% binder ($[CH_2C(CH_3)_2]_n$ polyisobuthylene/oppanol) solution in toluene (>99 %, Sigma-Aldrich). After 5 h of stirring, the slurry was casted on Al foil and

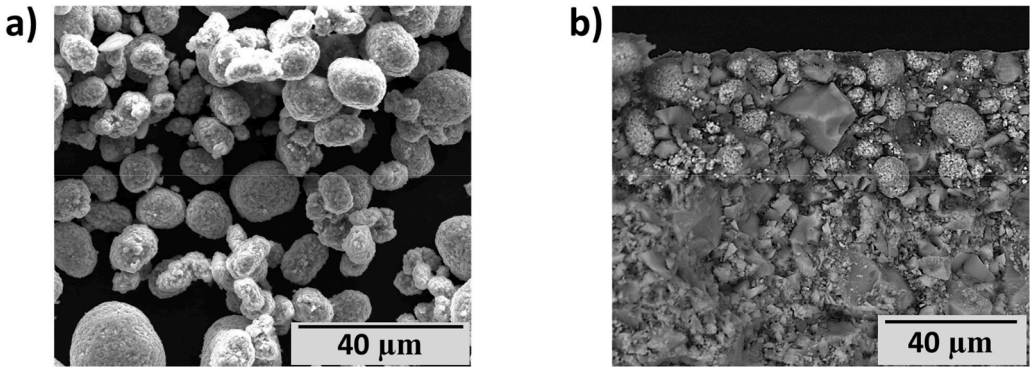


**Fig. 1.** SEM micrograph of NMC622 powder (**a**) and cross-section of the cathode/electrolyte interface acquired from a pristine bilayer (**b**).

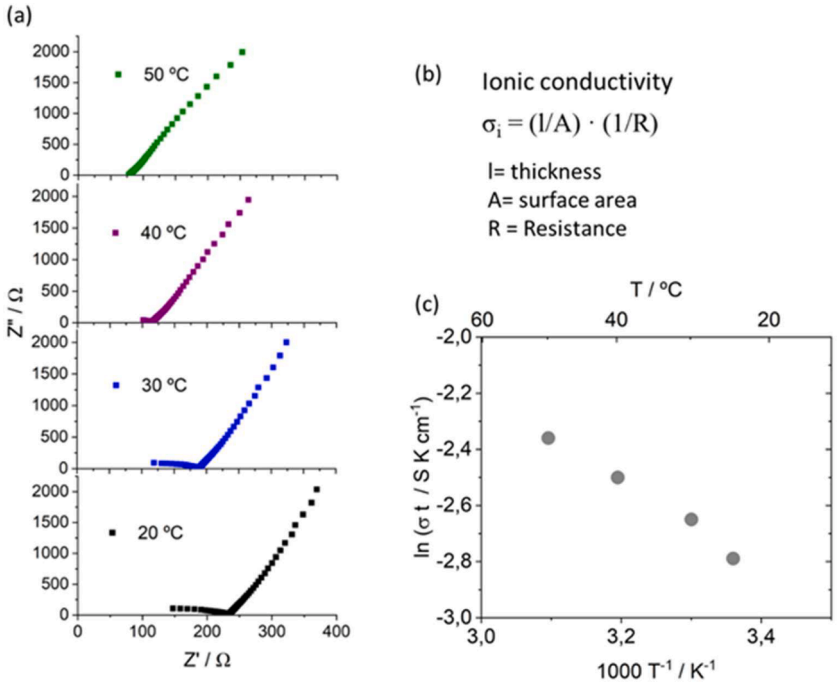


**Fig. 2.** (a) Nyquist plot of argyrodite electrolyte at different temperatures. (b) Equation of the ionic conductivity and (c) Arrhenius plot on the temperature range.

homogeneously spread over the surface using a Dr. Blade with a 250-300 µm gap. After drying under vacuum at room temperature for 15 h, cathode discs of Ø6 mm were punched and co-pressed with a densified SE pellet at 300–450-600 MPa, with 2 min of maintenance at each step. A final active mass loading of around 5 mg $cm^{-2}$ was obtained.

### 3.2. Electrochemical characterization

Electrochemical Impedance Spectroscopy (EIS) was performed to determine the ionic conductivity of the argyrodite electrolyte. Argyrodite pellet was densified under pressure and assembled between carbon coated aluminium foil. The cell was heated from 25 °C and up to 50 °C in

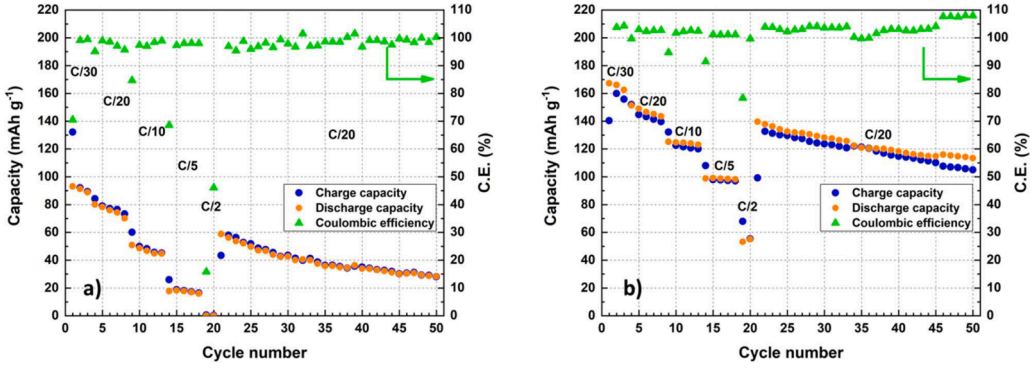


**Fig. 3.** Comparative rate capability for test (**a**) at 25 °C and (**b**) at 50 °C.

**Table 1**
Capacity retention of cell Li/$Li_6PS_5Cl$/NMC622.

| Cycle number | Capacity retention (Charge/Discharge capacity)% vs 2nd cycle (C/30) | |
|---|---|---|
| 3rd (C/30) | 97.45 | 97.92 |
| 8th (C/20) | 87.35 | 86.44 |
| 13th (C/10) | 75.13 | 74.11 |
| 18th (C/5) | 60.68 | 59.12 |
| 20th (C/2) | 34.59 | 33.20 |
| 25th (C/20) | 81.06 | 79.84 |
| 30th (C/20) | 77.33 | 77.18 |
| 35th (C/20) | 75.84 | 72.85 |
| 40th (C/20) | 71.76 | 71.28 |
| 45th (C/20) | 68.91 | 69.10 |
| 50th (C/20) | 65.67 | 68.30 |

a dynamic climate chamber (MKF 56, Binder). The Nyquist plots were recorded in a Solartron 1260A Impedance analyzer with frequencies ranging from 32 MHz to 1 Hz and a 50 mV excitation amplitude.

A BR-200 multi-channel Arbin Instrument was used to perform the galvanostatic cycling tests. LMBs were cycled in a potential window of 2.7–4.2 V vs Li/$Li^+$, in accordance with the stability limits for NMC622. Currents applied in the several charge/discharge cycles at different C-rates have been computed using a theoretical capacity of 165 mAh $g^{-1}$ and considering only the NMC active material of the electrode. [90] All the experiments were performed at 50 °C in a dynamic climate chamber (MKF 56, Binder).

### 3.3. Morphological analysis

The morphology of the NMC622 powder and the microstructure of cathode/electrolyte interface was studied by scanning electron microscopy (SEM) with a Quanta 200FEG electron microscope (Thermofischer), under an acceleration voltage of 20 kV, in the secondary or backscattered electrons mode. The cross-section micrographs of the cathode/electrolyte interface were acquired on fractured surfaces of a bilayer pellet.

## 4. Results and discussions

### 4.1. Experimental results

#### 4.1.1. Morphological analysis

The commercial NMC622 powder consists of 10-30 μm particles with a nearly spherical shape (Fig. 1a). The morphology of the active material is preserved in the cathode layer (Fig. 1b). The layer thickness is 40-50 μm, with an acceptable contact between the NMC622 and solid electrolyte phase, without visible porosity. The large diameter of NMC622 may result in an insufficient percolation between the NMC622 particles,

**Table 2**
Simulation electrochemical parameters.

| Parameter | Name | Negative electrode | SSE | Positive electrode | Aluminium |
|---|---|---|---|---|---|
| | | Design specifications (geometry and volume fraction) | | | |
| $A_{cell}$ ($m^2$) | Cell surface | 0.0000283 | | | |
| $L_i$ (μm) | Thickness | | 725 | 40 | |
| $R_i$ (μm) | Radius | | | 10 | |
| $\varepsilon_s$ | Porosity | | | 0.131 | |
| | | Lithium-ion concentration | | | |
| $c_{s,max}$ (mol $m^{-3}$) | Maximum molar concentration | | | 47,664[1] | |
| $c_{s,ini}$ (mol $m^{-3}$) | Initial molar concentration | | | 47,664[1] | |
| | | Kinetic and transport properties | | | |
| $\alpha_{a,i}$, $\alpha_{c,i}$ | Charge transfer coefficients | 0.5 | | 0.5 | |
| $\sigma_i$ (S $m^{-1}$) | Conductivity | | 0.43 | 0.17[1] | $3.77\times10^7$ |
| $D_i$ ($m^2$ $s^{-1}$) | Diffusion coefficient | | | $2\times10^{-13}$ | |
| | | Constant quantity | | | |
| T (K) | Temperature | 323.15 | | | |
| F (C $mol^{-1}$) | Faraday's constant | 96,487 | | | |
| R (J $mol^{-1}$ $K^{-1}$) | Universal gas constant | 8.314 | | | |

[1] COMSOL Multiphysics Library.

which is compensated by addition of electron-conductive C65.

#### 4.1.2. Electrochemical results

Electrochemical Impedance Spectroscopy (EIS) was performed to determine the ionic conductivity of the argyrodite electrolyte. Fig. 2 shows the Nyquist plot, the equation used to calculate the ionic conductivity and the Arrhenius plot. The argyrodite exhibits an ionic conductivity of 1.6 mS/cm at 25 °C and increases up to 4.3 mS/cm at 50 °C.

The rate capability of the NMC622 electrode with argyrodite SSE was assessed in the galvanostatic mode increasing the C-rates from C/30 to C/2, adopting the same C-rate both for charge and discharge. Three cycles at C/30, five cycles at C/20, C/10, C/5, and two cycles at C/2 have been considered. In the end, thirty cycles at C/20 have been applied with the purpose to assess the cell degradation at high C-rates. Furthermore, the effect of temperature on the cell performance has been studied cycling them at 25 °C and 50 °C. Fig. 3 reports the comparison between the cell cycled at 25 °C and 50 °C in terms of charge and discharge capacities and Coulombic efficiency for each cycle. In Fig. 3a, all the cycles show a poor performance in terms of charge and discharge capacity. The first three cycles display a charge/discharge capacity a little higher than half of the theoretical one. Then, the progressive increasing of the C-rates brings to a drastic reduction of the charge/

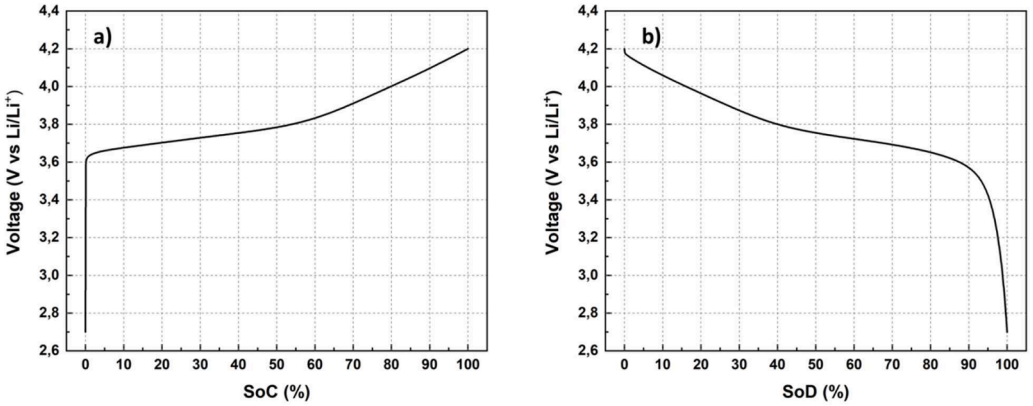


**Fig. 4.** Pseudo-OCV curves of NMC622: (**a**) as a function of the state of charge and (**b**) as a function of the state of discharge.

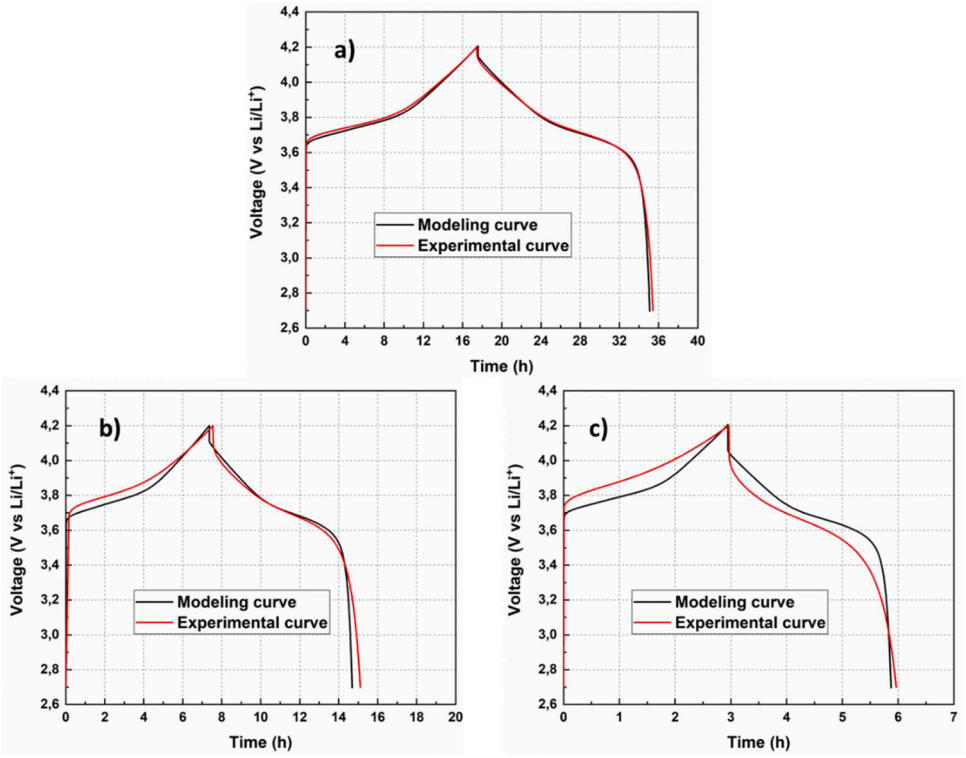


**Fig. 5.** a) Calibration of the modelling charge-discharge curves onto the experimental ones at C/20, Validation of the model by comparing modelled and experimental charge-discharge profiles at b) C/10, and c) C/5.

**Table 3**
Error values between model and experimental data.

| Cycle step | Error values for model-experiment | | |
|---|---|---|---|
| | C/20 | C/10 | C/5 |
| Charge capacity | 0.6 % | -2.4 % | -0.5 % |
| Discharge capacity | -2.5 % | -3.1 % | -2.6 % |

discharge capacity, that reaches 20 mAh $g^{-1}$ at C/5 and nearly no response at C/2. During the last cycling step at C/20 the cell partially recovers the capacity, delivering 60 mAh $g^{-1}$, that further drops down to 30 mAh $g^{-1}$ after 30 cycles. Such poor performances evidence kinetic issues stemming from the restricted ionic conductivity within the composite cathode at 25 °C, attributed to the presence of an insulating binder. Consequently, the cells were also cycled at 50 °C in order to increase the ionic conductivity of the solid electrolyte (from 1.6 mS/cm at 25 °C to 4.3 mS/cm at 50 °C as reported on Fig. 2) and to understand the aforementioned kinetic constrains (see Fig. 3b). The first three cycles show charge/discharge capacities similar to the NMC622 theoretical one (~165 mAh $g^{-1}$). The increasing of the C-rate brings to a progressive reduction of the practical charge/discharge capacities until C/5. For the two cycles at C/2, a sudden decrease can be observed: in fact, charge/discharge capacities just reach around 55 mAh $g^{-1}$ probably due to the too high overpotential at increased currents. However, coming back to C/20, the cell recovers a capacity as high as ~140 mAh $g^{-1}$, which agrees with ionic diffusion limitations rather than eventual chemical side reactions [91]. The influence of the latter is most probably the explanation for the capacity fade (from 140 mAh $g^{-1}$ to 115 mAh $g^{-1}$) observed in the last 30 cycles at C/20. Therefore, according to the better performances obtained at 50 °C, all the following experimental tests and discussions have been performed and studied at 50 °C.

For the cell cycled at 50 °C, the capacity retention has been computed for several cycles using as a reference the 2nd cycle (at C/30) charge/discharge capacities, due to the fact that the 2nd charge capacity is the highest value reached during the galvanostatic cycling. The values of charge/discharge capacity retention have been reported in Table 1: for the first 20 cycles, a similar capacity retention can be observed for charge and discharge. The increase of the C-rate, from C/5 to C/2, brings to a decrease of the capacity retention of 25 %, confirming again the poor electrochemical performances observed in the rate capability. In the last 30 cycles at C/20, the charge/discharge capacity retentions decrease with a quasi-linear behaviour, except for the last 5 cycles, where a higher reduction in charge capacity retention with respect to discharge can be noticed.

#### 4.1.3. Equilbrium potential curve

The cathode equilibrium potential curve is another useful electrochemical parameter that describes the P2D model. This curve represents voltage as a function of SoC or SoD (state of discharge), covering a potential window of 2.7–4.2 V vs. $Li/Li^+$. To get true OCV, galvanostatic cycling at a slow C-rate (C/30), known as pseudo-OCV, should be used. Therefore, the second cycle of rate capability of NMC622 at 50 °C has been considered.

During experimental characterization a polarization phenomenon was noticed between the cell charge and discharge, therefore both pseudo-OCV curves were implemented in the electrochemical model. Observing Fig. 4a and b for charge and discharge, respectively, the polarization phenomenon can be recognized. Considering, for both curves, a SoC equal to 50 %, a difference of 33 mV between the charge and discharge equilibrium voltage was calculated.

### 4.2. Calibration and validation of the electrochemical model

The P2D electrochemical model was calibrated in order to enhance the quality of the fitting between the simulated and the experimental charge-discharge curves at a fixed C-rate, in this case chosen equal to C/20. As described in previous sections, the fitting was achieved through experimental determination, such as average radius particle and open-circuit voltage. Table 2 reports the electrochemical parameters used to

develop the calibration model.

Subsequently, the validation of the electrochemical model was performed to prove the robustness and the consistency of the calibration of the P2D model, at C-rates different from the calibration one (C/20). The model was validated comparing one simulated charge-discharge cycle with the experimental one at the same C-rate. Because of the lower electrochemical performance obtained at C/2, this C-rate was excluded and only two different C-rates (C/10 and C/5) were considered for the validation. For the final validation, the charge-discharge current was the only electrochemical parameter changed in the calibrated model, according to the C-rate fixed. Fig. 5 shows the comparison at (a) C/20 for the calibration, (b) C/10, and (c) C/5 for the validation. It can be observed that all the experimental results are well fitted by the simulated curves, both for the required experimental charge-discharge times and for the electrochemical voltage behaviour. Some differences can be noticed at C/5 in terms of overpotentials, both in charge and discharge, probably caused by the interfacial resistance between the solid electrolyte and the electrodes. The errors between the capacities obtained from the model and the ones obtained experimentally were calculated and reported in Table 3. The errors have been computed as the percentage ratio between the difference of simulated and experimental capacities and the experimental capacities. All values are below 3.5 % confirming the strength of the P2D electrochemical model developed.

## 5. Conclusions

In this work, an innovative P2D electrochemical model for a metallic lithium – argyrodite $Li_6PS_5Cl$ – NMC622 cell was successfully developed. In particular, to the best of our knowledge, it is the first time that two important aspects characterizing this new battery generation were implemented together in a P2D model, against an NMC based cathode.

The first aspect is the implementation of solid-state electrolyte, in substitution of commercial liquid electrolyte. This has been possible through the use of the single ion conducting electrolyte theory, according to which Ohm's law is the only equation to be solved in the electrolyte domain. In fact, it can be highlighted that, while the electrochemical parameters characterizing the equation of the current density in a liquid electrolyte (concentrated solution theory) are three (the electrolyte conductivity, the transference number, and the mean molar activity coefficient), one parameter is enough to characterize a SSE, thus representing a further simplification of the P2D model, as well as a reduced number of experimental measurements to obtain the necessary parameters.

The second one regards the substitution of graphite by lithium metal, implying a different treatment from an electrochemical point of view. Indeed, while graphite was a porous, intercalating electrode, metallic lithium can be simply considered an infinite lithium reservoir and therefore as a boundary condition.

The developed P2D model is able to fit properly the cell electrochemical behaviour at two different C-rates (C/10, C/5). This result was obtained thanks to a careful calibration work, which allowed to extract important electrochemical parameters, such as OCV curves, through experimental measurements. Such procedure increases the electrochemical model accuracy making it as realistic as possible, as demonstrated in the validation phase.

The obtained model adequately describes the experimental results at low currents, whereas at higher currents and overpotentials a more complex model could be required, to take into account the interfacial resistance associated with insufficient mechanical contact as well as other factors.

Keeping in mind that ASSBs are not usually tested at high C-rates and considering the low computational cost of the simulation as well as the accuracy obtained studying the combination of metallic lithium and solid-state electrolyte, the model reported here could be a simple and adaptable tool for future analysis. As a matter of fact, other SSEs, such as oxides-based, could be considered within a similar P2D electrochemical model simply measuring and modifying a single electrochemical parameter: the ionic conductivity of the solid-state electrolyte.

In conclusion, the implementation of solid-state electrolyte in combination with metallic lithium in a P2D model, thus resulting in its simplification, could be a suitable strategy to further the understanding of this promising battery technology, thus contributing to its future upscaling.

## Funding information

The presented work was supported by the European Commission through the H2020 program under Grant agreement number 875028 (SUBLIME Project).

## Declaration of competing interest

The authors declare that they have no known competing financial interests or personal relationships that could have appeared to influence the work reported in this paper.

## Data availability

Data will be made available on request.

## Acknowledgments

The presented work was supported by the European Commission through the H2020 program under Grant agreement number 875028 (SUBLIME Project).

## References

[1] H. Matalata, S. Syafii, M.I. Hamid, Evaluation of Future Battery Electric Vehicles as an Environmentally Friendly Transportation Means: a Review, Andalasian International Journal of Applied Science, Engineering and Technology 3 (2023) 32–43, https://doi.org/10.25077/aijaset.v3i01.67.

[2] M. Gutsch, J. Leker, Global warming potential of lithium-ion battery energy storage systems: a review, J. Energy Storage 52 (2022) 105030, https://doi.org/10.1016/j.est.2022.105030.

[3] L. Al-Ghussain, Global warming: review on driving forces and mitigation, Environ. Prog. Sustain. Energy 38 (2019) 13–21, https://doi.org/10.1002/ep.13041.

[4] S. Sarmah, B.K.Kakati Lakhanlal, D. Deka, Recent advancement in rechargeable battery technologies, WIREs Energy and Environment 12 (2023), https://doi.org/10.1002/wene.461.

[5] R. Wang, W. Cui, F. Chu, F. Wu, Lithium metal anodes: present and future, J. Energy Chem. 48 (2020) 145–159, https://doi.org/10.1016/J.JECHEM.2019.12.024.

[6] N. Nitta, F. Wu, J.T. Lee, G. Yushin, Li-ion battery materials: present and future, Materials Today 18 (2015) 252–264, https://doi.org/10.1016/j.mattod.2014.10.040.

[7] A. Mayyas, K. Moawad, A. Chadly, E. Alhseinat, Can circular economy and cathode chemistry evolution stabilize the supply chain of Li-ion batteries? Extr. Ind. Soc. 14 (2023) 101253 https://doi.org/10.1016/j.exis.2023.101253.

[8] S.S. Ravi, M. Aziz, Utilization of Electric Vehicles for Vehicle-to-Grid Services: progress and Perspectives, Energies. (Basel) 15 (2022) 589, https://doi.org/10.3390/en15020589.

[9] H. Yuan, X. Ding, T. Liu, J. Nai, Y. Wang, Y. Liu, C. Liu, X. Tao, A review of concepts and contributions in lithium metal anode development, Materials Today 53 (2022) 173–196, https://doi.org/10.1016/j.mattod.2022.01.015.

[10] D. Lin, Y. Liu, Y. Cui, Reviving the lithium metal anode for high-energy batteries, Nat. Nanotechnol. 12 (2017) 194–206, https://doi.org/10.1038/nnano.2017.16.

[11] J.-F. Ding, Y.-T. Zhang, R. Xu, R. Zhang, Y. Xiao, S. Zhang, C.-X. Bi, C. Tang, R. Xiang, H.S. Park, Q. Zhang, J.-Q. Huang, Review on lithium metal anodes towards high energy density batteries, Green Energy & Environment (2022), https://doi.org/10.1016/J.GEE.2022.08.002.

[12] B. Liu, J.G. Zhang, W. Xu, Advancing Lithium Metal Batteries, Joule 2 (2018) 833–845, https://doi.org/10.1016/J.JOULE.2018.03.008.

[13] B. Li, Y. Wang, S. Yang, A Material Perspective of Rechargeable Metallic Lithium Anodes, Adv. Energy Mater. 8 (2018) 1702296, https://doi.org/10.1002/aenm.201702296.

[14] M. Zhao, B.-Q. Li, X.-Q. Zhang, J.-Q. Huang, Q. Zhang, A Perspective toward Practical Lithium–Sulfur Batteries, ACS. Cent. Sci. 6 (2020) 1095–1104, https://doi.org/10.1021/acscentsci.0c00449.

[15] J.-H. Kang, J. Lee, J.-W. Jung, J. Park, T. Jang, H.-S. Kim, J.-S. Nam, H. Lim, K. R. Yoon, W.-H. Ryu, I.-D. Kim, H.R. Byon, Lithium–Air Batteries: air-Breathing

Challenges and Perspective, ACS. Nano 14 (2020) 14549–14578, https://doi.org/10.1021/acsnano.0c07907.
[16] J. Xiang, Y. Wei, Y. Zhong, Y. Yang, H. Cheng, L. Yuan, H. Xu, Y. Huang, Building Practical High-Voltage Cathode Materials for Lithium-Ion Batteries, Advanced Materials 34 (2022) 2200912, https://doi.org/10.1002/adma.202200912.
[17] J. Amici, C.A. Calderón, D. Versaci, G. Luque, D. Barraco, E. Leiva, C. Francia, S. Bodoardo, Composite polymer electrolyte with high inorganic additive contents to enable metallic lithium anode, Electrochim. Acta 404 (2022), https://doi.org/10.1016/j.electacta.2021.139772.
[18] Y. Han, B. Liu, Z. Xiao, W. Zhang, X. Wang, G. Pan, Y. Xia, X. Xia, J. Tu, Interface issues of lithium metal anode for high-energy batteries: challenges, strategies, and perspectives, InfoMat 3 (2021) 155–174, https://doi.org/10.1002/inf2.12166.
[19] X.-B. Cheng, R. Zhang, C.-Z. Zhao, Q. Zhang, Toward Safe Lithium Metal Anode in Rechargeable Batteries: a Review, Chem. Rev. 117 (2017) 10403–10473, https://doi.org/10.1021/acs.chemrev.7b00115.
[20] B. Li, Y. Chao, M. Li, Y. Xiao, R. Li, K. Yang, X. Cui, G. Xu, L. Li, C. Yang, Y. Yu, D. P. Wilkinson, J. Zhang, A Review of Solid Electrolyte Interphase (SEI) and Dendrite Formation in Lithium Batteries, Electrochem. Energ. Rev. 6 (2023) 7, https://doi.org/10.1007/s41918-022-00147-5.
[21] Y. TAKEDA, O. YAMAMOTO, N. IMANISHI, Lithium Dendrite Formation on a Lithium Metal Anode from Liquid, Polymer and Solid Electrolytes, Electrochemistry 84 (2016) 210–218, https://doi.org/10.5796/electrochemistry.84.210.
[22] Q. Wang, B. Liu, Y. Shen, J. Wu, Z. Zhao, C. Zhong, W. Hu, Confronting the Challenges in Lithium Anodes for Lithium Metal Batteries, Adv. Sci. 8 (2021), https://doi.org/10.1002/advs.202101111.
[23] Q. Wang, B. Liu, Y. Shen, J. Wu, Z. Zhao, C. Zhong, W. Hu, Confronting the Challenges in Lithium Anodes for Lithium Metal Batteries, Adv. Sci. 8 (2021) 2101111, https://doi.org/10.1002/advs.202101111.
[24] S. Li, M. Jiang, Y. Xie, H. Xu, J. Jia, J. Li, Developing High-Performance Lithium Metal Anode in Liquid Electrolytes: challenges and Progress, Advanced Materials 30 (2018) 1706375, https://doi.org/10.1002/adma.201706375.
[25] H. Adenusi, G.A. Chass, S. Passerini, K.V. Tian, G. Chen, Lithium Batteries and the Solid Electrolyte Interphase (SEI)—Progress and Outlook, Adv. Energy Mater. (2023) 2203307, https://doi.org/10.1002/aenm.202203307.
[26] C. Fang, X. Wang, Y.S. Meng, Key Issues Hindering a Practical Lithium-Metal Anode, Trends. Chem. 1 (2019) 152–158, https://doi.org/10.1016/j.trechm.2019.02.015.
[27] H. Yuan, G. Zheng, D. Zhang, X. Yang, Review on Action Mechanism and Characterization of Natural/Artificial Solid Electrolyte Interphase of Lithium Battery: latest Progress and Future Directions, Energy & Fuels 37 (2023) 833–857, https://doi.org/10.1021/acs.energyfuels.2c02920.
[28] D. Kang, M. Xiao, J.P. Lemmon, Artificial Solid-Electrolyte Interphase for Lithium Metal Batteries, Batter. Supercaps. 4 (2021) 445–455, https://doi.org/10.1002/batt.202000225.
[29] L. Li, H. Dai, C. Wang, Electrolyte additives: adding the stability of lithium metal anodes, Nano Select 2 (2021) 16–36, https://doi.org/10.1002/nano.202000164.
[30] Q. Ma, J. Cui, J. Luo, A. Dong, Nonreactive Electrolyte Additives for Stable Lithium Metal Anodes, ACS. Appl. Energy Mater. 5 (2022) 3–13, https://doi.org/10.1021/acsaem.1c03333.
[31] S. Li, Z. Luo, L. Li, J. Hu, G. Zou, H. Hou, X. Ji, Recent progress on electrolyte additives for stable lithium metal anode, Energy Storage Mater. 32 (2020) 306–319, https://doi.org/10.1016/j.ensm.2020.07.008.
[32] J. Li, Z. Kong, X. Liu, B. Zheng, Q.H. Fan, E. Garratt, T. Schuelke, K. Wang, H. Xu, H. Jin, Strategies to anode protection in lithium metal battery: a review, InfoMat 3 (2021) 1333–1363, https://doi.org/10.1002/inf2.12189.
[33] L. Zhai, K. Yang, F. Jiang, W. Liu, Z. Yan, J. Sun, High-performance solid-state lithium metal batteries achieved by interface modification, J. Energy Chem. 79 (2023) 357–364, https://doi.org/10.1016/j.jechem.2023.01.022.
[34] D. Karabelli, K.P. Birke, M. Weeber, A Performance and Cost Overview of Selected Solid-State Electrolytes: race between Polymer Electrolytes and Inorganic Sulfide Electrolytes, Batteries. (Basel) 7 (2021) 18, https://doi.org/10.3390/batteries7010018.
[35] R. Wei, S. Chen, T. Gao, W. Liu, Challenges, fabrications and horizons of oxide solid electrolytes for solid-state lithium batteries, Nano Select 2 (2021) 2256–2274, https://doi.org/10.1002/nano.202100110.
[36] W. Zhao, J. Yi, P. He, H. Zhou, Solid-State Electrolytes for Lithium-Ion Batteries: fundamentals, Challenges and Perspectives, Electrochem. Energ. Rev. 2 (2019) 574–605, https://doi.org/10.1007/s41918-019-00048-0.
[37] S. Liang, W. Yan, X. Wu, Y. Zhang, Y. Zhu, H. Wang, Y. Wu, Gel polymer electrolytes for lithium ion batteries: fabrication, characterization and performance, Solid. State Ion. 318 (2018) 2–18, https://doi.org/10.1016/j.ssi.2017.12.023.
[38] F. Baskoro, H.Q. Wong, H.-J. Yen, Strategic Structural Design of a Gel Polymer Electrolyte toward a High Efficiency Lithium-Ion Battery, ACS. Appl. Energy Mater. 2 (2019) 3937–3971, https://doi.org/10.1021/acsaem.9b00295.
[39] W. Li, Y. Pang, J. Liu, G. Liu, Y. Wang, Y. Xia, A PEO-based gel polymer electrolyte for lithium ion batteries, RSC. Adv. 7 (2017) 23494–23501, https://doi.org/10.1039/C7RA02603J.
[40] C. Ma, W. Cui, X. Liu, Y. Ding, Y. Wang, In situ preparation of gel polymer electrolyte for lithium batteries: progress and perspectives, InfoMat 4 (2022), https://doi.org/10.1002/inf2.12232.
[41] M. Zhu, J. Wu, Y. Wang, M. Song, L. Long, S.H. Siyal, X. Yang, G. Sui, Recent advances in gel polymer electrolyte for high-performance lithium batteries, J. Energy Chem. 37 (2019) 126–142, https://doi.org/10.1016/j.jechem.2018.12.013.
[42] M.V. Reddy, C.M. Julien, A. Mauger, K. Zaghib, Sulfide and Oxide Inorganic Solid Electrolytes for All-Solid-State Li Batteries: a Review, Nanomater. 10 (2020) 1606, https://doi.org/10.3390/nano10081606.
[43] Y. Ren, K. Chen, R. Chen, T. Liu, Y. Zhang, C.-W. Nan, Oxide Electrolytes for Lithium Batteries, J. American Ceramic Soci. 98 (2015) 3603–3623, https://doi.org/10.1111/jace.13844.
[44] Y. Deng, C. Eames, B. Fleutot, R. David, J.-N. Chotard, E. Suard, C. Masquelier, M. S. Islam, Enhancing the Lithium Ion Conductivity in Lithium Superionic Conductor (LISICON) Solid Electrolytes through a Mixed Polyanion Effect, ACS. Appl. Mater. Interfaces. 9 (2017) 7050–7058, https://doi.org/10.1021/acsami.6b14402.
[45] K. Yang, L. Chen, J. Ma, Y. He, F. Kang, Progress and perspective of Li $_{1+}$ <scp>$_{x}$ Al $_{x}$ Ti $_{2}$ </scp>$_{-x}$ (<scp>PO $_{4}$ </scp>) $_{3}$ ceramic electrolyte in lithium batteries, InfoMat 3 (2021) 1195–1217, https://doi.org/10.1002/inf2.12222.
[46] J.D. LaCoste, A. Zakutayev, L. Fei, A Review on Lithium Phosphorus Oxynitride, The J. Phys. Chem. C 125 (2021) 3651–3667, https://doi.org/10.1021/acs.jpcc.0c10001.
[47] H. Su, Z. Jiang, Y. Liu, J. Li, C. Gu, X. Wang, X. Xia, J. Tu, Recent progress of sulfide electrolytes for all-solid-state lithium batteries, Energy Materials (2022), https://doi.org/10.20517/energymater.2022.01.
[48] S. Chen, D. Xie, G. Liu, J.P. Mwizerwa, Q. Zhang, Y. Zhao, X. Xu, X. Yao, Sulfide solid electrolytes for all-solid-state lithium batteries: structure, conductivity, stability and application, Energy Storage Mater. 14 (2018) 58–74, https://doi.org/10.1016/j.ensm.2018.02.020.
[49] W.G. Suci, H.K.(Kiwi) Aliwarga, Y.R. Azinuddin, R.B. Setyawati, K.N.R. Stulasti, A. Purwanto, Review of various sulfide electrolyte types for solid-state lithium-ion batteries, Open Engineering 12 (2022) 409–423, https://doi.org/10.1515/eng-2022-0043.
[50] J. Wu, L. Shen, Z. Zhang, G. Liu, Z. Wang, D. Zhou, H. Wan, X. Xu, X. Yao, All-Solid-State Lithium Batteries with Sulfide Electrolytes and Oxide Cathodes, Electrochem. Energ. Rev. 4 (2021) 101–135, https://doi.org/10.1007/s41918-020-00081-4.
[51] A. Kraytsberg, Y. Ein-Eli, Recent Developments in the Field of Sulfide Ceramic Solid-State Electrolytes, Energy Technology (2023) 2201291, https://doi.org/10.1002/ente.202201291.
[52] B. Tao, C. Ren, H. Li, B. Liu, X. Jia, X. Dong, S. Zhang, H. Chang, Thio-/LISICON and LGPS-Type Solid Electrolytes for All-Solid-State Lithium-Ion Batteries, Adv. Funct. Mater. 32 (2022) 2203551, https://doi.org/10.1002/adfm.202203551.
[53] Y. Liang, H. Liu, G. Wang, C. Wang, Y. Ni, C. Nan, L. Fan, Challenges, interface engineering, and processing strategies toward practical <scp>sulfide-based all-solid-state</scp>lithium batteries, InfoMat 4 (2022) 66, https://doi.org/10.1002/inf2.12292.
[54] Y.-W. Byeon, H. Kim, Review on Interface and Interphase Issues in Sulfide Solid-State Electrolytes for All-Solid-State Li-Metal Batteries, Electrochem 2 (2021) 452–471, https://doi.org/10.3390/electrochem2030030.
[55] J. Zhang, C. Zheng, L. Li, Y. Xia, H. Huang, Y. Gan, C. Liang, X. He, X. Tao, W. Zhang, Unraveling the Intra and Intercycle Interfacial Evolution of Li $_{6}$ PS $_{5}$ Cl-Based All-Solid-State Lithium Batteries, Adv. Energy Mater. 10 (2020), https://doi.org/10.1002/aenm.201903311.
[56] J. Janek, W.G. Zeier, Challenges in speeding up solid-state battery development, Nat. Energy 8 (2023) 230–240, https://doi.org/10.1038/s41560-023-01208-9.
[57] R. Chen, Q. Li, X. Yu, L. Chen, H. Li, Approaching Practically Accessible Solid-State Batteries: stability Issues Related to Solid Electrolytes and Interfaces, Chem. Rev. 120 (2020) 6820–6877, https://doi.org/10.1021/acs.chemrev.9b00268.
[58] Y. Xia, J. Li, J. Zhang, X. Zhou, H. Huang, X. He, Y. Gan, Z. Xiao, W. Zhang, Yttrium stabilized argyrodite solid electrolyte with enhanced ionic conductivity and interfacial stability for all-solid-state batteries, J. Power. Sour. 543 (2022) 231846, https://doi.org/10.1016/j.jpowsour.2022.231846.
[59] Y. Xia, J. Li, Z. Xiao, X. Zhou, J. Zhang, H. Huang, Y. Gan, X. He, W. Zhang, Argyrodite Solid Electrolyte-Integrated Ni-Rich Oxide Cathode with Enhanced Interfacial Compatibility for All-Solid-State Lithium Batteries, ACS. Appl. Mater. Interfaces. 14 (2022) 33361–33369, https://doi.org/10.1021/acsami.2c08940.
[60] Y.-Y. Sun, Q. Zhang, L. Yan, T.-B. Wang, P.-Y. Hou, A review of interfaces within solid-state electrolytes: fundamentals, issues and advancements, Chemical Engineering Journal 437 (2022) 135179, https://doi.org/10.1016/j.cej.2022.135179.
[61] H.M. Woolley, N.M. Vargas-Barbosa, Hybrid solid electrolyte-liquid electrolyte systems for (almost) solid-state batteries: why, how, and where to? J. Mater. Chem. a Mater. 11 (2023) 1083–1097, https://doi.org/10.1039/D2TA02179J.
[62] Q. Ye, X. Li, W. Zhang, Y. Xia, X. He, H. Huang, Y. Gan, X. Xia, J. Zhang, Slurry-Coated LiNi $_{0.8}$ Co $_{0.1}$ Mn $_{0.1}$ O $_{2}$ –Li $_{3}$ InCl $_{6}$ Composite Cathode with Enhanced Interfacial Stability for Sulfide-Based All-Solid-State Batteries, ACS. Appl. Mater. Interfaces. 15 (2023) 18878–18888, https://doi.org/10.1021/acsami.3c00178.
[63] X. Li, Q. Ye, Z. Wu, W. Zhang, H. Huang, Y. Xia, Y. Gan, X. He, X. Xia, J. Zhang, High-voltage all-solid-state lithium batteries with Li3InCl6 electrolyte and LiNbO3 coated lithium-rich manganese oxide cathode, Electrochim. Acta 453 (2023) 142361, https://doi.org/10.1016/j.electacta.2023.142361.
[64] K.G. Naik, B.S. Vishnugopi, J. Datta, D. Datta, P.P. Mukherjee, Electro-Chemo-Mechanical Challenges and Perspective in Lithium Metal Batteries, Appl. Mech. Rev. 75 (2023), https://doi.org/10.1115/1.4057039.
[65] Z. Wu, X. Li, C. Zheng, Z. Fan, W. Zhang, H. Huang, Y. Gan, Y. Xia, X. He, X. Tao, J. Zhang, Interfaces in Sulfide Solid Electrolyte-Based All-Solid-State Lithium Batteries: characterization, Mechanism and Strategy, Electrochem. Energ. Rev. 6 (2023) 10, https://doi.org/10.1007/s41918-022-00176-0.
[66] V.S. Deshpande, R.M. McMeeking, Models for the Interplay of Mechanics, Electrochemistry, Thermodynamics, and Kinetics in Lithium-Ion Batteries, Appl. Mech. Rev. 75 (2023), https://doi.org/10.1115/1.4056289.

[67] D. Miranda, R. Gonçalves, S. Wuttke, C.M. Costa, S. Lanceros-Méndez, Overview on Theoretical Simulations of Lithium-Ion Batteries and Their Application to Battery Separators, Adv. Energy Mater. 13 (2023), https://doi.org/10.1002/aenm.202203874.
[68] A. Orue Mendizabal, M. Cheddadi, A. Tron, A. Beutl, P. López-Aranguren, Understanding Interfaces at the Positive and Negative Electrodes on Sulfide-Based Solid-State Batteries, ACS. Appl. Energy Mater. (2023), https://doi.org/10.1021/acsaem.3c01894.
[69] J. Schmitt, I. Horstkötter, B. Bäker, Electrical lithium-ion battery models based on recurrent neural networks: a holistic approach, J. Energy Storage 58 (2023) 106461, https://doi.org/10.1016/j.est.2022.106461.
[70] F. Brosa Planella, W. Ai, A.M. Boyce, A. Ghosh, I. Korotkin, S. Sahu, V. Sulzer, R. Timms, T.G. Tranter, M. Zyskin, S.J. Cooper, J.S. Edge, J.M. Foster, M. Marinescu, B. Wu, G. Richardson, A continuum of physics-based lithium-ion battery models reviewed, Progress in Energy 4 (2022) 042003, https://doi.org/10.1088/2516-1083/ac7d31.
[71] Y. Sun, T. Yang, H. Ji, J. Zhou, Z. Wang, T. Qian, C. Yan, Boosting the Optimization of Lithium Metal Batteries by Molecular Dynamics Simulations: a Perspective, Adv. Energy Mater. 10 (2020) 2002373, https://doi.org/10.1002/aenm.202002373.
[72] W. Chen, Y. Li, D. Feng, C. Lv, H. Li, S. Zhou, Q. Jiang, J. Yang, Z. Gao, Y. He, J. Luo, Recent progress of theoretical research on inorganic solid state electrolytes for Li metal batteries, J. Power. Sources. 561 (2023) 232720, https://doi.org/10.1016/j.jpowsour.2023.232720.
[73] Y. Li, L. Sha, G. Zhang, B. Chen, W. Zhao, Y. Wang, S. Shi, Phase-field simulation tending to depict practical electrodeposition process in lithium-based batteries, Chinese Chemical Letters 34 (2023) 107993, https://doi.org/10.1016/j.cclet.2022.107993.
[74] L. Xu, X. Lin, Y. Xie, X. Hu, Enabling high-fidelity electrochemical P2D modeling of lithium-ion batteries via fast and non-destructive parameter identification, Energy Storage Mater. 45 (2022) 952–968, https://doi.org/10.1016/J.ENSM.2021.12.044.
[75] Z. Chen, D.L. Danilov, R. Eichel, P.H.L. Notten, Porous Electrode Modeling and its Applications to Li-Ion Batteries, Adv. Energy Mater. 12 (2022) 2201506, https://doi.org/10.1002/aenm.202201506.
[76] M. Doyle, T.F. Fuller, J. Newman, Modeling of Galvanostatic Charge and Discharge of the Lithium/Polymer/Insertion Cell, J. Electrochem. Soc. 140 (1993) 1526–1533, https://doi.org/10.1149/1.2221597.
[77] A.A. Wang, S.E.J. O'Kane, F. Brosa Planella, J.Le Houx, K. O'Regan, M. Zyskin, J. Edge, C.W. Monroe, S.J. Cooper, D.A. Howey, E. Kendrick, J.M. Foster, Review of parameterisation and a novel database (LiionDB) for continuum Li-ion battery models, Progress in Energy 4 (2022) 032004, https://doi.org/10.1088/2516-1083/ac692c.
[78] P. Hashemzadeh, M. Désilets, M. Lacroix, A. Jokar, Investigation of the P2D and of the modified single-particle models for predicting the nonlinear behavior of Li-ion batteries, J. Energy Storage 52 (2022) 104909, https://doi.org/10.1016/j.est.2022.104909.
[79] K. Liu, Y. Gao, C. Zhu, K. Li, M. Fei, C. Peng, X. Zhang, Q.L. Han, Electrochemical modeling and parameterization towards control-oriented management of lithium-ion batteries, Control Eng Pract 124 (2022), https://doi.org/10.1016/J.CONENGPRAC.2022.105176.
[80] D. Dessantis, P. Di Prima, D. Versaci, J. Amici, C. Francia, S. Bodoardo, M. Santarelli, Aging of a Lithium-Metal/LFP Cell: predictive Model and Experimental Validation, Batteries. (Basel) 9 (2023) 146, https://doi.org/10.3390/batteries9030146.
[81] R. Franke-Lang, J. Kowal, Electrochemical Model-Based Investigation of Thick LiFePO4 Electrode Design Parameters, Modelling 2 (2021) 259–287, https://doi.org/10.3390/modelling2020014.
[82] K. Kumaresan, Y. Mikhaylik, R.E. White, A Mathematical Model for a Lithium–Sulfur Cell, J. Electrochem. Soc. 155 (2008) A576, https://doi.org/10.1149/1.2937304.
[83] T. Zhang, M. Marinescu, S. Walus, G.J. Offer, Modelling transport-limited discharge capacity of lithium-sulfur cells, Electrochim. Acta 219 (2016) 502–508, https://doi.org/10.1016/J.ELECTACTA.2016.10.032.
[84] U. Sahapatsombut, H. Cheng, K. Scott, Modelling the micro-macro homogeneous cycling behaviour of a lithium-air battery, J. Power. Sources. 227 (2013) 243–253, https://doi.org/10.1016/j.jpowsour.2012.11.053.
[85] U. Sahapatsombut, H. Cheng, K. Scott, Modelling of operation of a lithium-air battery with ambient air and oxygen-selective membrane, J. Power. Sour.. 249 (2014) 418–430, https://doi.org/10.1016/J.JPOWSOUR.2013.10.128.
[86] N. Wolff, F. Röder, U. Krewer, Model Based Assessment of Performance of Lithium-Ion Batteries Using Single Ion Conducting Electrolytes, Electrochim. Acta 284 (2018) 639–646, https://doi.org/10.1016/j.electacta.2018.07.125.
[87] A. Tron, R. Hamid, N. Zhang, A. Beutl, Rational Optimization of Cathode Composites for Sulfide-Based All-Solid-State Batteries, Nanomaterials 13 (2023) 327, https://doi.org/10.3390/nano13020327.
[88] Y.J. Heo, S. Seo, S. Hwang, S.H. Choi, D. Kim, One-pot aprotic solvent-enabled synthesis of superionic <scp>Li-argyrodite</scp>solid electrolyte, Int. J. Energy Res. 46 (2022) 17644–17653, https://doi.org/10.1002/er.8324.
[89] D. Liu, Y. He, Y. Chen, J. Cao, F. Zhu, Electrochemical modeling, Li plating onsets and performance analysis of thick graphite electrodes considering the solid electrolyte interface formed from the first cycle, Electrochim. Acta. 439 (2023) 141651, https://doi.org/10.1016/j.electacta.2022.141651.
[90] X. Pan, H. Sun, Z. Wang, H. Huang, Q. Chang, J. Li, J. Gao, S. Wang, H. Xu, Y. Li, W. Zhou, High Voltage Stable Polyoxalate Catholyte with Cathode Coating for All-Solid-State Li-Metal/NMC622 Batteries, Adv. Energy Mater. 10 (2020) 2002416, https://doi.org/10.1002/aenm.202002416.
[91] A.H. Dao, P. López-Aranguren, J. Zhang, F. Cuevas, M. Latroche, Solid-State Li-Ion Batteries Operating at Room Temperature Using New Borohydride Argyrodite Electrolytes, Mater. (Basel) 13 (2020) 4028, https://doi.org/10.3390/ma13184028.